Photon Counting and Fast Photometry with L3 CCDs

Simon Tulloch
Isaac Newton Group of Telescopes, Apartado 321, Santa Cruz de La Palma,
Islas Canarias, 38700, SPAIN

ABSTRACT

The new L3 Technology CCDs from E2V allow detector read noise to be decoupled from readout speed. If operated at sufficiently high gain, the read noise drops to sub-electron levels and photon counting becomes possible. At ING we have incorporated CCD60 , CCD87 and CCD97 L3 detectors into cryogenic cameras coupled to SDSU controllers for a variety of tests both in the lab and on-sky using the 4.2m William Herschel Telescope. These detectors have been operated in proportional and photon-counting mode using an in-house Linux based DAS. We have gained a number of insights into photon counting optimisation, how to cope with the effects of the L3 pipeline delay and the reduction of internal device-generated spurious charge. We have also discovered a statistical method for determining the gain of an L3 system from pulse height analysis of the individual photon events. Our on-sky test program has consisted to date of high frame rate photometry of the Crab Nebula Pulsar.

Keywords: L3 CCD Fast Photometry Photon Counting ING

1. INTRODUCTION

1.1 Multiplication Process

In a conventional CCD the pixel charge packets exiting the serial register dump directly onto the output node where they are sensed by a MOSFET transistor. With the E2V Technologies L3 CCDs each pixel leaving the serial register instead passes through a novel 520 stage 'multiplication register' on its way to the output node. A high voltage clock on one of the phases of this register creates avalanche multiplication so that each input photo-electron reaches the output node as a large charge packet that renders the intrinsic amplifier noise insignificant. Single photo-electrons can therefore be easily detected and amplifier noise becomes decoupled from readout speed to a large extent. A large gain in SNR is achieved at low signal levels using L3 technology, however, at higher signal levels where a conventional CCD will be photon noise dominated, L3 technology can actually give a root2 reduction in SNR due to the statistics of the multiplication process. This reduction in SNR is commonly termed 'multiplication noise'.

1.2 The Two Modes of Operation

These are Proportional Mode (PPM) and Photon Counting Mode (PCM). They only differ in the way in which the pixel data is interpreted, although PCM will generally use a much higher gain, controllable easily by tuning the amplitude of the HV multiplication clock. In PPM, the pixel data is interpreted conventionally as representing so many photo-electrons per ADU. Flat field images analysed in this mode will have a sigma proportional to the mean signal , *not* proportional to the root of the mean as in conventional photon statistics: a manifestation of the multiplication noise. In PCM the pixel values are instead thresholded and if they exceed a certain value they are interpreted as representing single photo-electrons. This will only work at low illumination levels otherwise co-incidence losses will reduce the effective QE of the detector. Using PCM removes multiplication noise and the final processed images will obey conventional photon statistics.

2. TEST CAMERA DESIGN

2.1 Camera Controller

A modified SDSU II controller was used for characterisation of the L3 CCDs. A variable multiplication clock amplitude of between 20 and 45V was required for the L3 register and this is not available using a standard controller. Instead , an E2V high voltage clock module was purchased and adapted to fit inside the SDSU.

2.2 Test Cryostats

Two cryogenic cameras were built and are shown below in figures 1. and 2. The first uses the 128 pixel square CCD60, the second uses either the CCD87 or CCD97 512 pixel square detectors which are plug compatible. Connections between the CCDs and the hermetic connector were direct and unshielded. A 50cm shielded cable connected camera and controller.

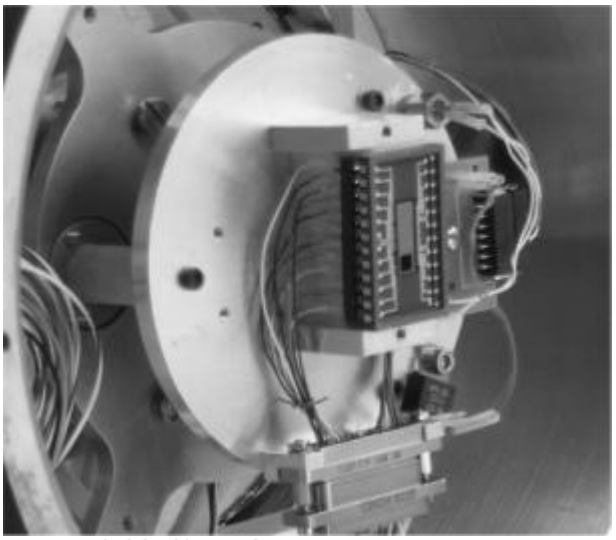

Fig. 1. ING CCD60 Test Camera

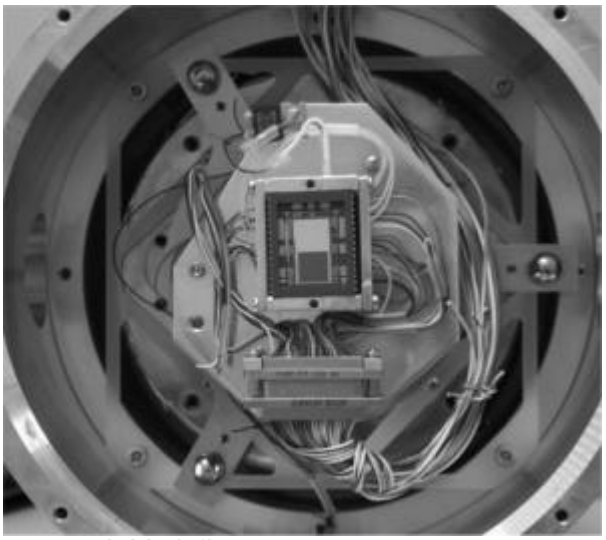

Fig. 2. ING CCD87/97 test camera

Some additional data was obtained using a cryogenic CCD97 camera developed by the University of Cambridge

3. L3 CCD CHARACTERISTICS

3.1 Multiplication Noise

This is fundamental and unavoidable. Fig. 3. below shows L3 photon statistics at various exposure and gain levels.

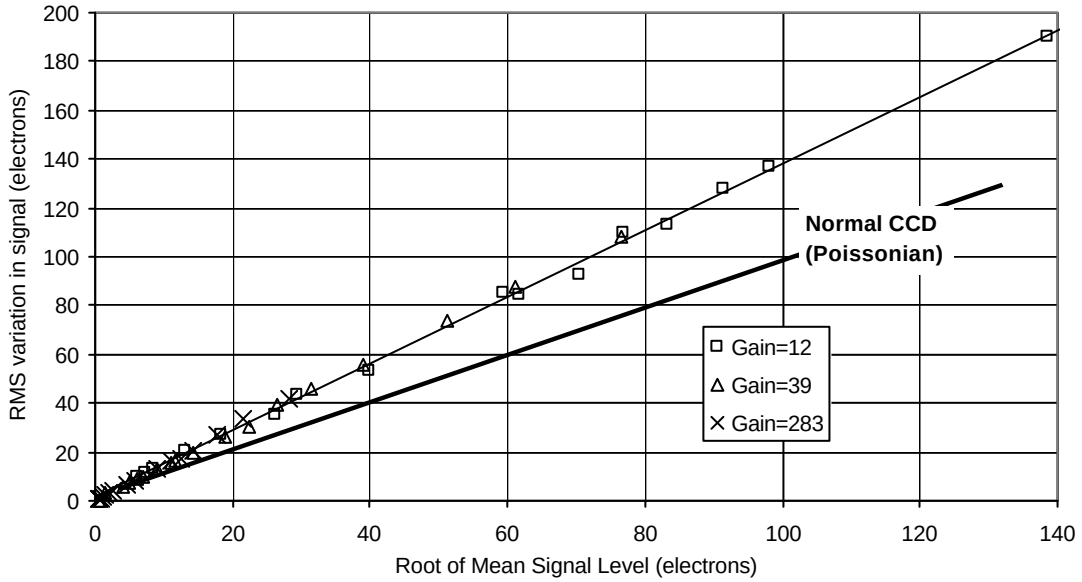

Fig. 3. Photon transfer graph using CCD60 L3 CCD data. Normal CCD response shown for comparison.

The standard photon-transfer gain measurement technique which relies on comparing mean signal levels with their standard deviations must be modified with L3 CCDs. The actual gain , as measured in input electrons per ADU, will be twice the traditionally measured photon-transfer value.

3.2 Amplifier Glow

Dark frames taken with the CCD87 showed a glow originating in the lower left hand corner. It could be largely removed by dropping the Output Drain (OD) of the on-chip FET during integration. The area illuminated by this glow was remarkable in that it extended *under* the shield of the store section. Another weakly illuminated area can be seen at the lower left of the image area, here the illumination path was by reflection from the aluminium plate used to clamp the CCD onto its cold finger. A 180s CCD87 dark frame is shown below in Fig. 4.

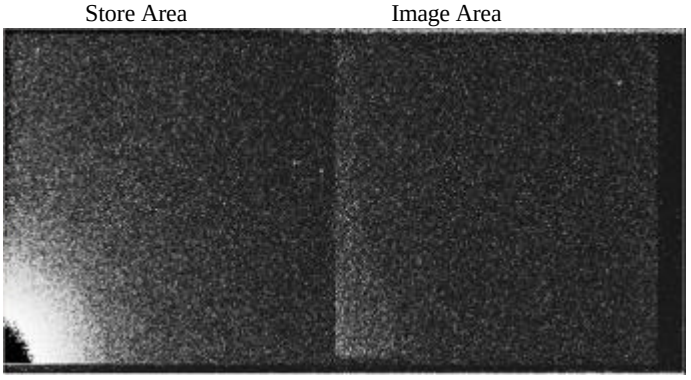

Fig. 4. CCD87 amplifier glow

It was also found necessary to keep the OD low even when idling since amplifier glow seemed to cause a remnance effect lasting tens of seconds in the CCD. Even once these precautions had been followed, amplifier glow was still visible at a low level if many bias frames were summed. During readout the pixels will unavoidably pass close to the fully powered-on output FET and be exposed to stray photons for the duration of the line-readout time. Fig. 5. shows the sum of 50 CCD97 dark frames The line-readout time in this image was 2ms. Notice that the right hand side of the image appears brighter. The adjacent dark strip is the serial overscan region. The same effect could still be seen in a much faster system operating at 260us per line. The CCD97 was specially engineered to reduce amplifier glow and number of stray photons was tiny , however, this could still be significant if these detectors are to be used for photon counting.

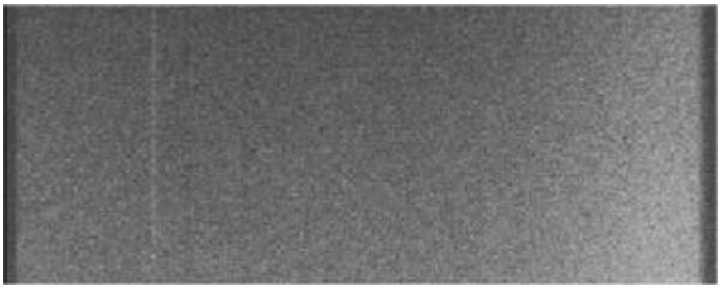

Fig. 5. Low level amplifier glow visible in CCD97

3.3 Clock Induced Charge (CIC)

This was found to be the dominant noise source in L3 CCDs. The clocking of the CCD during readout can itself generate electrons, which in the case of those arising from the vertical clocks are indistinguishable from true photo-

electrons. Spurious charge is also found in conventional CCDs but is rarely a problem except when they are highly binned. Janesick [1] states that CIC is caused by positive going clock edges taking a clock phase out of inversion, that it increases exponentially with clock swing and decreases exponentially with clock rise time. Further he states that the CIC increases at lower temperatures and is proportional to the time the clocks stay out of inversion. The CIC was measured for the L3 CCDs by summing a large number of bias images. The system gain was then calibrated using weakly illuminated flat fields (for exact method see Sec 3.5). Furthermore, histograms of the CIC events in image and serial overscan regions were compared in an effort to understand the exact origin of the charge. The CIC from the ING CCD60/87/97 cameras was unfortunately very high, of the order of 0.1e per pixel. The readout rate during the measurements was 250Kpix/s. Careful examination of the summed biases showed no difference in level between the serial and parallel overscan regions indicating that the source of the stray charge was either the serial or L3 register. Examination of the pixel value histogram further narrowed down the source as being the L3 register. This is shown below in Fig. 6. where the actual pixel histogram of a series of CCD87 bias images is compared with the output of two Monte Carlo (MC) models.

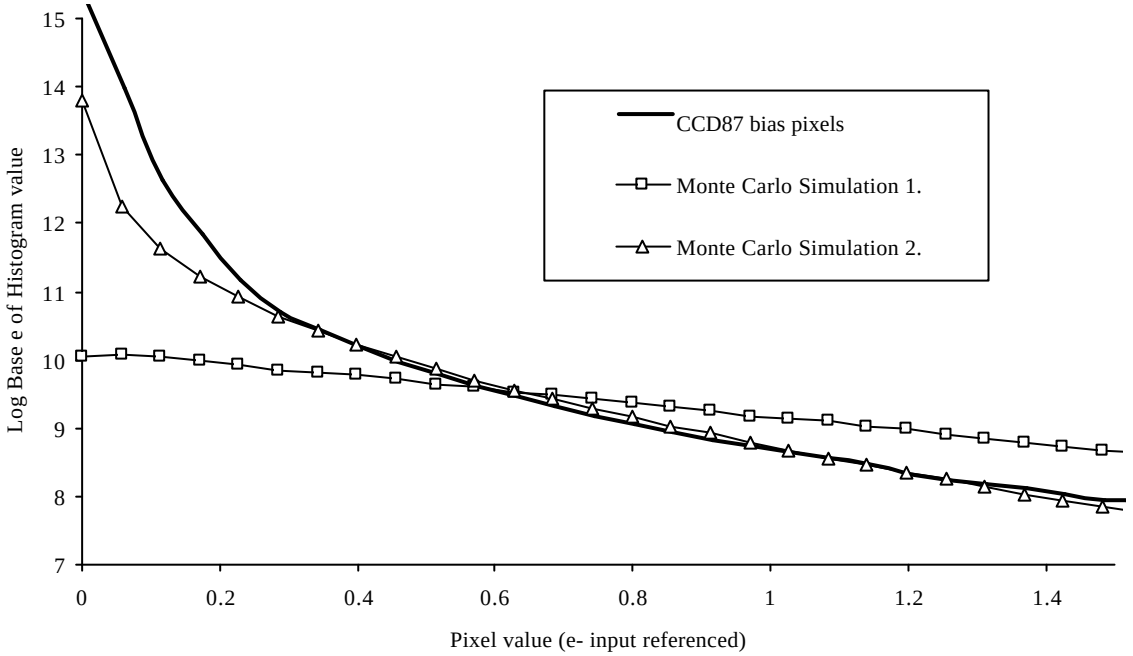

MC Model 1: Expected histogram from an ideal flat field exposure of 1 photo-electron per image area pixel.
MC Model 2: Expected histogram from a bias exposure with CIC generated at random positions along L3 register

Fig. 6. CIC histogram using CCD87 data compared with two Monte Carlo models.

Model 2 assumed that each pixel had a probability of 0.3 of receiving a spurious electron whilst traversing the L3 register. The actual bias histogram showed an excess of low value counts since most of the CIC will be subject to less than 520 stages of L3 amplification, depending on the position that it is generated . The fit is quite good except at the low end. The excess of actual pixel values here, compared to the model, could be explained by deferred charge from the less than perfect horizontal charge transfer (see Sec. 3.4).

Further data was supplied by the University of Cambridge Institute of Astronomy who run a cryogenic CCD97 at a pixel rate of 4MHz using an AstroCam 4100 Capella controller. Their images show remarkably low CIC, approximately 0.004 e- per pixel . This seems to be generated in equal proportions by the serial/L3 and parallel clocks. Fig. 7. shows a mean line profile through approximately 160 bias frames. These images contained 560 columns of serial overscan and because of the L3 pipeline this appears to the left of the image area.

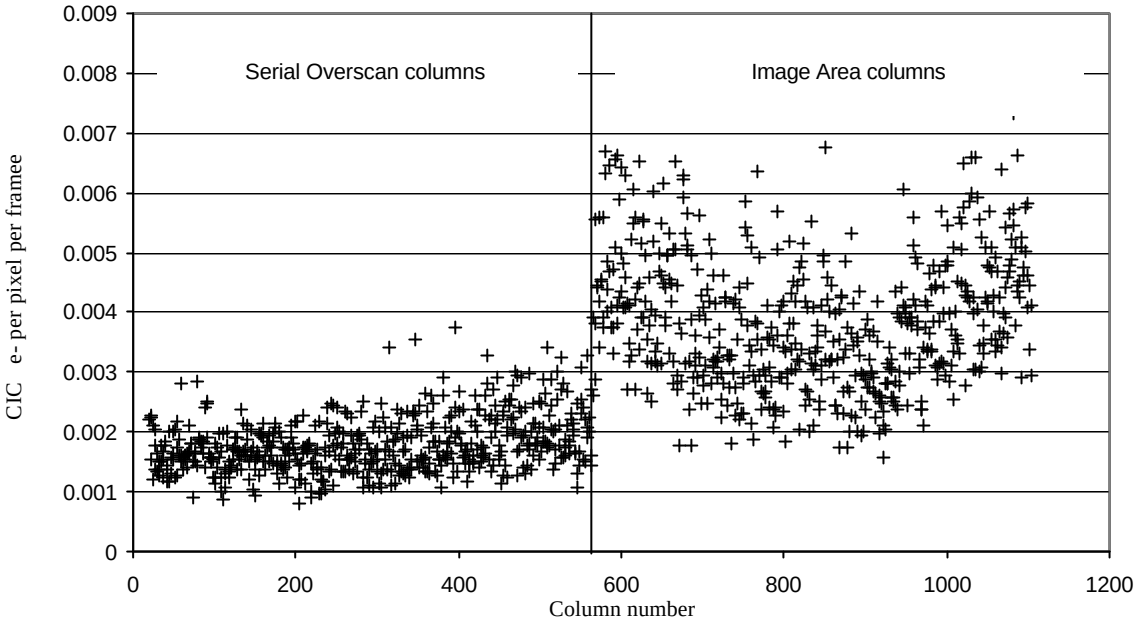

Fig. 7. CIC in the Cambridge CCD97 camera.

The graph is in rough agreement with the expectations of E2V i.e. approximately 1 in 500 pixels of CIC. The slight increase at the edges of the image area (where the parallel clocks will be faster) suggests that a further reduction could be achieved by slowing down the parallel clock edges. The differences between the ING and Cambridge data (a factor of 50 in CIC) are probably related to differences in the clock timings and the cleanliness of the clock edges. Ringing edges could be particularly effective at generating CIC. It should be noted that the effects of CIC are very different from that of Gaussian read noise in a standard CCD. CIC is more akin to a faint 'spiky' background pedestal.

3.4 Charge Transfer Efficiency (CTE)

This was studied using the Fe55 X-ray technique and faint cosmetic defects on an engineering grade CCD87. The X-ray technique showed good horizontal charge transfer efficiency in the vertical and horizontal clocks. Fig. 8. shows the X-ray event values as a function of column number. Multiplication noise has broadened the X-ray line but it is still obviously close to horizontal indicating good HCTE. The faint defect on the chip, however, showed a large horizontal tail, visible in Fig. 9, somewhat in contradiction to the earlier result. This conflict can be explained by poor HCTE in the L3 multiplication register only. The deferred charge from the defect amounted to 14% ; corresponding to a CTE of 0.9997 per transfer within the L3 register. Another heavily exposed Airy disc image (Fig. 14.) shows a large tail of deferred charge stretching across hundreds of columns. The tail 'wraps round' into the next image line where it appears to the left of the over-exposed spot. Poor CTE gives an effect similar to CIC, in that it distributes stray 'left-over' electrons along the L3 register where they constitute a small additional noise source. The measurements were performed at 160K. A similar CTE result was obtained for the CCD60 using the Extended Pixel Edge Response (EPER) technique. The CCD87 has dark reference columns to left and right of the image area which are defined with an aluminium mask. These gave a soft edge to the image area so the EPER technique could not be used.

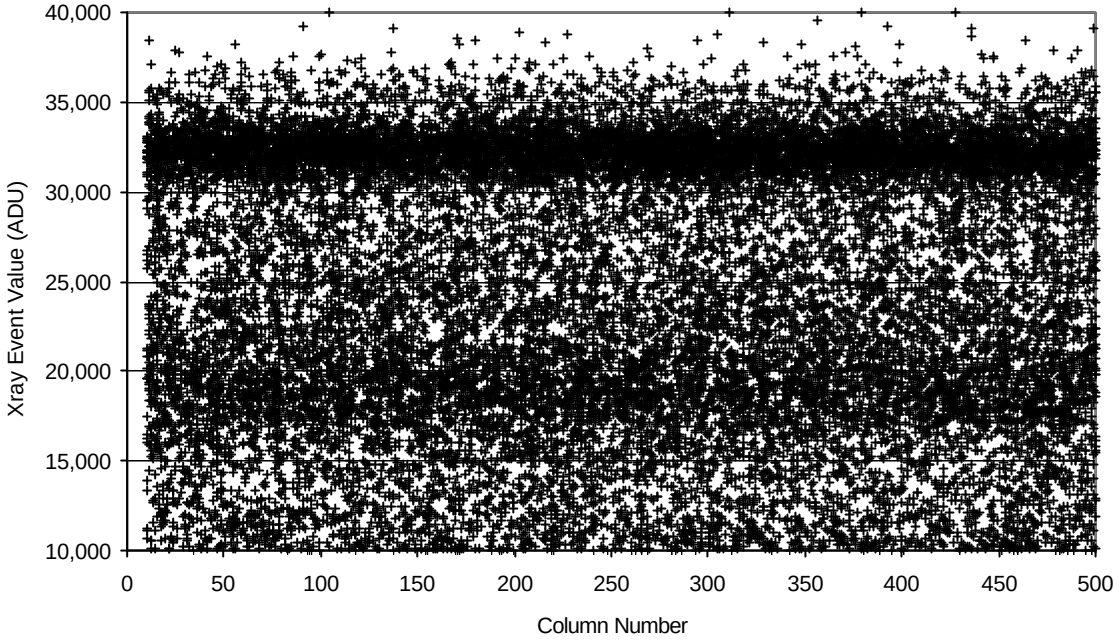

Fig. 8. CCD87 Fe55 X-ray CTE plot

Fig. 9. Imperfect HCTE in CCD87 highlighted by a faint defect (image was read out to the right in this illustration).

3.5 L3 Gain Measurement Technique

If the histogram of a very low illumination flat field are taken, (i.e. one where coincidence losses are negligible, say 0.1 photons per pixel) the histogram takes the form of an inverse exponential. If the vertical axis of the histogram is then plotted on a Natural Logarithmic scale, the slope of the histogram will then be equal to –1 x the gain, the gain being expressed as input referenced photo-electrons per ADU. This is demonstrated in Fig. 10. for two different gain values. Data at low signal values was not used in the line fitting since it represents CIC and not true photo-electron events. Gaussian noise from the output FET could also cause a low level histogram excess but in this instance it was only at the 3 ADU level and would fall entirely within the first histogram bin.

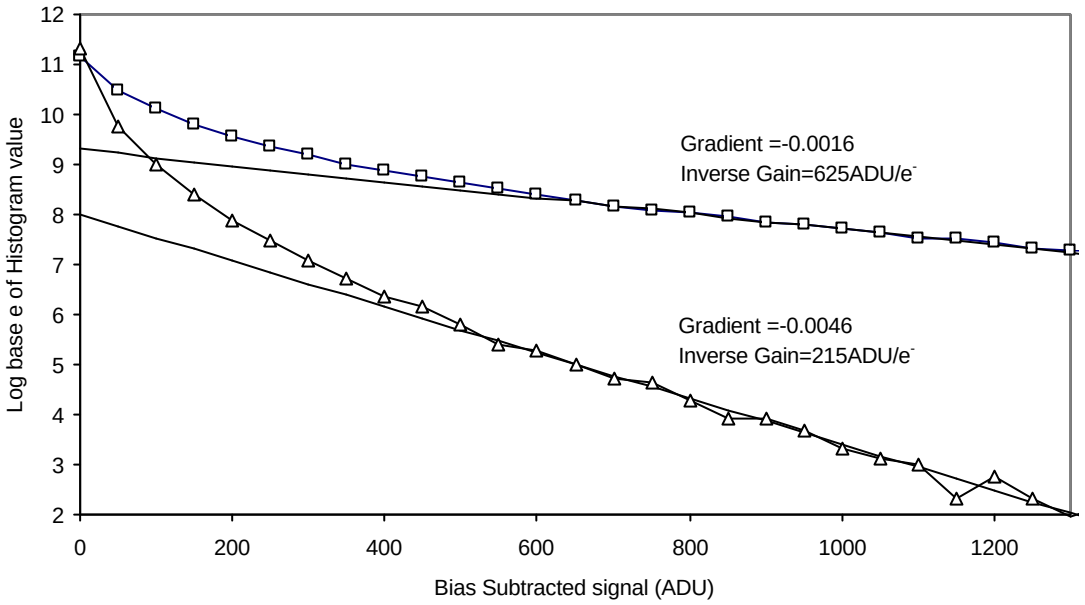

Fig. 10. Photon event histograms used to measure L3 gain.

This technique is particularly useful for device characterisation since gain can vary greatly with only small variations in temperature and multiplication clock amplitude.

3.6 L3 Pipeline Delay

The L3 devices studied all have a 520 stage multiplication stage. In the case of the CCD60, there are an additional 24 passive stages in the pipeline giving a total delay of 544 pixels. For the CCD87/97 the total delay is 560 pixels. This produces a 1 line pipeline delay in the case of the CCD87/97 and a 4 line delay in the case of the CCD60. This pipeline must be filled prior to the start of video ADC pixel transmission. If it is not then the first lines will either contain garbage, or in the case of TV style readout, pixels from the previous frame. With the SDSU controller there is an additional 3 pixel internal pipeline delay in the ADC. This is fairly straightforward to deal with until variable windowing is required. Cosmetic problems arise if a vertical transfer occurs half way through a line readout. In normal CCD operation this will not occur but with a pipeline delay it can. To reach a window it is necessary to first skip over the pixels to its left, then read normally the pixels in the window and then finally either skip over the remaining pixels to the right of the window or do a serial register dump using the Dump Gate (DG). This latter option can speed up operation since it reduces the number of serial transfers but can also cause pipeline problems. If the DG option is used and the skip width + the window width are not an integral fraction of the pipeline length, there will be a bias discontinuity in mid-image. This is illustrated in Fig. 11. where the discontinuity is visible between the first two columns of Shack Hartmann spots.

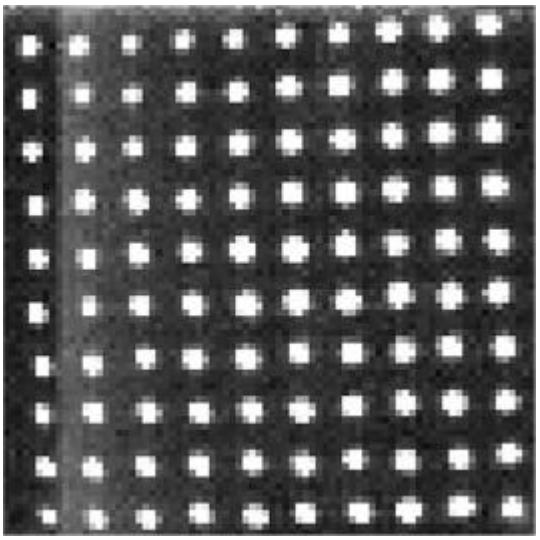

Fig. 11. Bias discontinuity as a side effect of the pipeline delay in a CCD60

4. PHOTON COUNTING PERFORMANCE

4.1 Choice of Threshold Value

Photon counting is attractive in low signal environments because it eliminates the multiplication noise. The choice of photon counting threshold turns out to be very important. Simply setting it at the $1e^-$ level (input referenced) will only catch e^{-1} (approximately 37%) of the photo-electrons ; remember that the output histogram of single electron events follows an inverse exponential. Fig. 12. shows how the detected fraction of photon events falls as the threshold is raised. With the threshold at $0.1e^-$, 90% of the photo-electrons will be detected. Decreasing below this increases the risk of false triggers due to EMI and intrinsic amplifier noise.

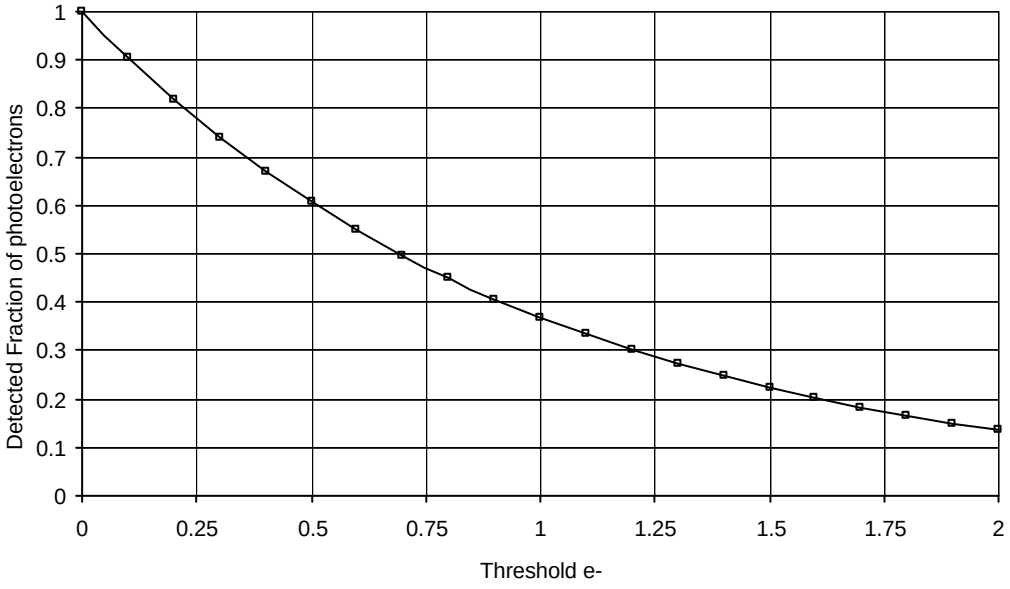

Fig. 12. Photon counting efficiency as a function of threshold level.

None of the cameras tested were really capable of photon counting performance. In the case of the ING cameras the limitation was the high CIC that restricted the operation to a very narrow range of illuminations. In the case of the Cambridge camera, the limitation was the very high intrinsic amplifier noise which prevents a usefully low photon counting threshold being used. Fig 13. compares two of the cameras tested.

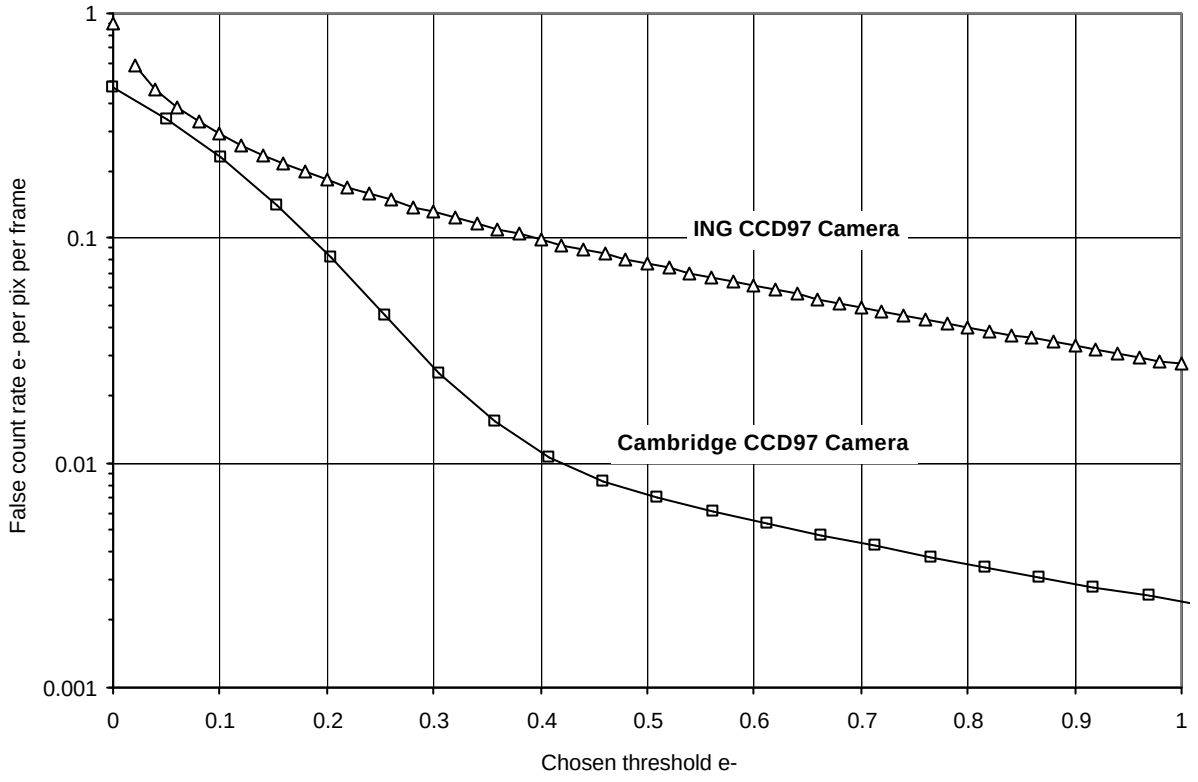

Fig. 13. Relationship between false trigger rate and photon counting threshold for two L3 cameras.

5. PROPORTIONAL MODE PERFORMANCE

All the cameras tested gave good PM performance with sub-electron noise. In the case of the ING cameras the noise was limited by the CIC, in the case of the Cambridge camera it was limited by intrinsic amplifier noise due to the fast pixel rate. The effective read noise levels are tabulated below.

Camera	Effective Read Noise in PM
ING CCD60	0.2e
ING CCD97	0.2e
ING CCD87	0.07e
Cambridge CCD97	0.15e

6. L3 CCD OBSERVATIONS.

6.1 Photon Diffraction

This was a nice demonstration of wave-particle duality. A 20um pinhole was placed just in front of the camera window and monochromatically illuminated with a weak distant source. A large series of short images were recorded. This stack was then bias subtracted and thresholded to yield the photon events which were accumulated to create the output image.

This is shown in Fig 14. alongside one of the raw input frames. A movie showing the gradual build-up of this image is available on the ING web site[2].

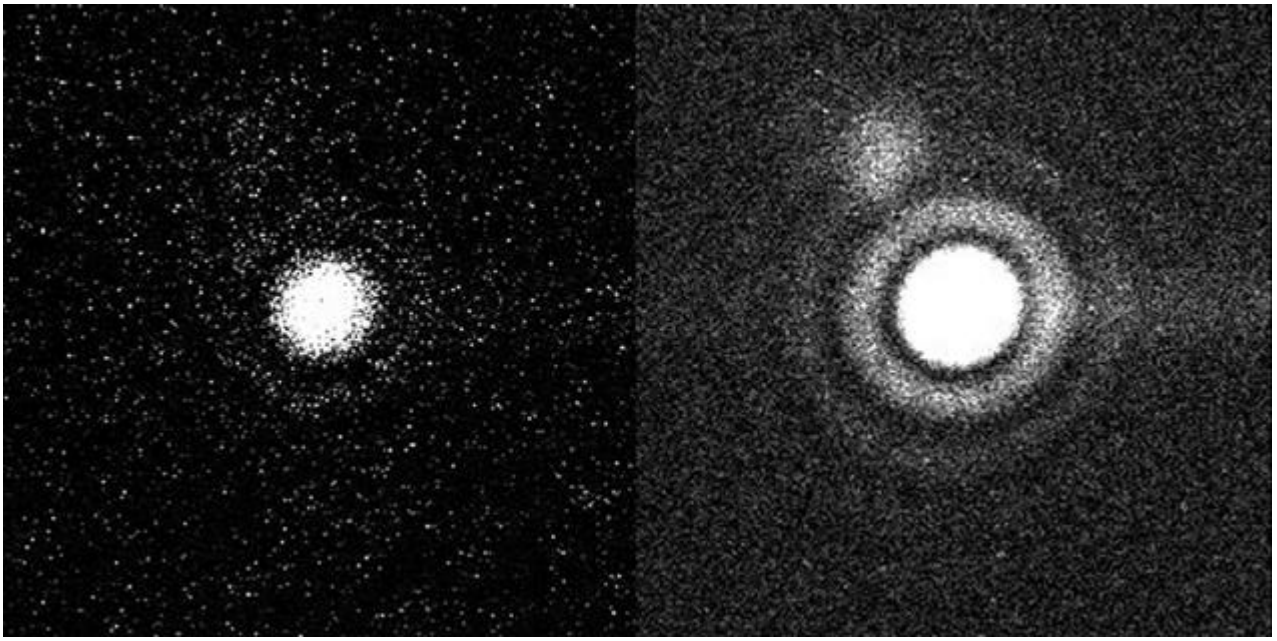

Fig. 14. Photon diffraction as demonstrated with the CCD87. One raw input image shown on left. Photon counted sum of 50 raw frames shown on right.

6.2. High Speed Photometry of the Crab Nebula Pulsar

The Crab Pulsar flashes at 29.9Hz and is an ideal target for demonstrating high speed photometry. The peak brightness is M_v12. The pulsar was observed using the CCD60 test camera on the auxiliary imaging port of the William Herschel Telescope. The frame rate was 180Hz. The camera was operated in frame transfer mode so that it was continuously exposing even during readout. Normally it is necessary to phase-bin many images to bring out the periodicity of this source , however, with the CCD60 the flashes were directly visible in the raw frames. A burst of 1000 frames was recorded of which a small section is shown in Fig. 15. Frame number 3, measured from the left, even shows the weak secondary pulse of this object.

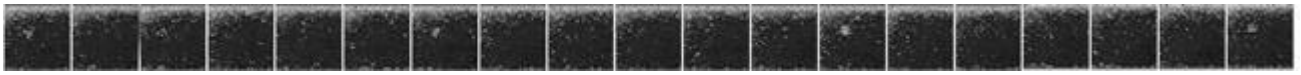

Fig. 15. Three cycles of the Crab Nebula Pulsar observed with the ING CCD60 camera.

The total duration of the exposure burst was enough to record 166 pulsar periods. Not all of these were visible and it is thought that the short section shown above shows a brief period of low Seeing. Here the image width was 0.3-0.4", in other sections of the 'movie strip' Seeing had spread the pulsar out over too many pixels for it to be so clearly visible. The complete sequence is shown on the ING web site[3] . This technique of 'Lucky Astronomy' that takes advantage of Seeing windows to achieve AO type performance, is currently being pursued by a group from the University of Cambridge [4].

7. CONCLUSIONS

L3 CCDs give a large SNR improvement under low levels of illumination. They decouple to a large extent read noise and readout speed and are therefore ideal for high speed photometric observations, one very promising application being wavefront sensing. They also have potential as photon counting detectors although none of the cameras tested here performed efficiently in this mode. The clock waveforms must be very carefully set-up to obtain optimum performance. Horizontal charge transfer is lower than for conventional CCDs and this could be a problem for some applications.

ACKNOWLEDGEMENTS

Thanks to Paul Jorden and Benjamin Hadwen of E2V technologies for provision of test CCDs and additional information on L3 technology. Thanks also to Craig Mackay of the University of Cambridge for providing CCD97 image data.

REFERENCES

1. Janesick, Scientific Charge Coupled Devices, p649
2. Photon Diffraction Movie: http://www.ing.iac.es/~smt/counting/movie.htm
3. Crab Pulsar Movie: http://www.ing.iac.es/~smt/WFS/pulsar.htm
4. Lucky Imaging URL: http://www.ast.cam.ac.uk/~optics/Lucky_Web_Site/index.htm

ING L3 URL: http://www.ing.iac.es/~smt/LLLCCD/marcl3.htm